CERN–ACC–2019–0001
Stefano.Redaelli@cern.ch

Staged implementation of low–impedance collimation in IR7: plans for LS2

S. Antipov, N. Biancacci, A. Bertarelli, R. Bruce, F. Carra, G. Gobbi, A. Lechner, A. Mereghetti, E. Métral, S. Redaelli, B. Salvant
CERN, Geneva, Switzerland

Abstract

The HL–LHC upgrade baseline foresees to replace all secondary collimators of IR7 until LS3 in order to ensure a sufficient margin for beam stability with the high–brightness upgraded beams. The present TCSG design is based on a carbon–fibre composite (CFC) material and will be replaced with a new low–impedance design (TCSPM). The TCSPM design is based on a Molybdenum–Graphite (MoGr) composite material coated with pure Molybdenum. These collimators also embed in–jaw beam position monitors (BPMs) for a fast alignment and local orbit monitoring as well as an additional BPM for measurements of the orbit transverse to the collimation plane. A staged deployment strategy of the low–impedance upgrade is proposed that foresees to install 4 TCSPM collimators per beam in LS2 and the remaining 7 in LS3. In this note, the slots to be equipped with the TCSPM in LS2 are defined.

Geneva, Switzerland
January 30, 2019

Contents

1 Introduction **3**

2 Present layouts and installation constraints **4**

3 Highlights of TCSPM design **6**

4 Comparative assessment of alternative layouts **9**
4.1 General considerations 9
4.2 Considered layout configurations 14
4.3 Impedance contributions 14
4.4 Beam loss simulations 18
4.5 Thermo–mechanical response to steady beam losses 22

5 Proposed baseline solution **26**

6 Conclusions **27**

1 Introduction

The low–impedance upgrade of the LHC collimation system [1] is necessary to ensure with sufficient margins the stability of the HL–LHC high–brightness beams [2], of intensity nearly doubled compared to that of the present LHC. From the impedance and beam instability point of view, the goal of the upgrade is to replace those collimators in IR7 which dominate the impedance contribution from collimators, to achieve on paper a stabilising octupole current which is a factor $\sim$2 lower than the maximum available octupole current [2]. Such a margin is deemed necessary in order to compensate for other sources of beam instability which emerged in past years of LHC operation like external noise injected into the beam (e.g. via ADT, power converters, etc. . .). These sources have been spot in measurements in recent years, showing that they can lead to beam instability [3]; nevertheless, scaling laws are presently not clear and will be investigated in the coming years. From the robustness point of view, the new collimators should withstand the increased loads induced by the brighter HL–LHC beams; in particular, maximum loss rates will double, as a result of the doubled bunch intensity for the same minima of beam lifetime with respect to nominal LHC design figures [1].

The collimation upgrade foresees to replace all the 22 secondary collimators of the betatron cleaning insertion (IR7), called TCSG, with new ones with a new design, called TCSPM. The new design is based on an active part made of molybdenum–graphite (MoGr) coated with Mo that replaces the present design based on carbon–fibre composite (CFC). In addition, the new design includes two in–jaw beam position monitors (BPMs) for the collimator alignment, and a new third BPM that enables measuring the orbit in the plane orthogonal to the collimation plane. A new design of the transitions at the jaw extremities that house the BPMs is also implemented. A drawing of the TCSPM design is shown in Fig. 1. Details of other design improvements can be found in [4].

Our project strategy is to pursue a staged deployment of the low–impedance collimators, consisting of two phases: a first installation in the Long Shutdown 2 (LS2, in the period 2019–2020) followed by a second installation in LS3, in 2023–2024 [2]. This approach has various advantages. It already provides an important reduction of the collimator impedance for the LHC Run III, when the upgraded beam parameters from the LHC Injector Upgrade (LIU) program will progressively become available. This will provide important benefits to the LHC operation and will allow studying better the possible impedance limitations. In addition, a staged deployment allows possible further iterations on the new collimator design for the second production line for LS3. The staged approach also allows distributing resources that would otherwise have to be made available in LS3, when various other parallel activities for different HL–LHC upgrades will be on–going, in particular the collimation upgrade of the high–luminosity inser-

tions IR1 and IR5 [2].

For an optimum deployment of low–impedance collimators in Run III, various studies were carried out to identify the IR7 secondary collimator slots to be upgraded with highest priority. This analysis starts with an assessment of the slots that contribute most to the collimator impedance, but also includes other considerations related to the overall performance of the collimation system. After a brief recap of the present layouts in IR7, which also addresses the constraints that have to be taken into account, the design of the TCSPM collimator is reviewed. Different possible layouts are then comparatively assessed for the post–LS2 LHC running configuration. Based on the outcome of these studies, a baseline solution is proposed and conclusions are drawn.

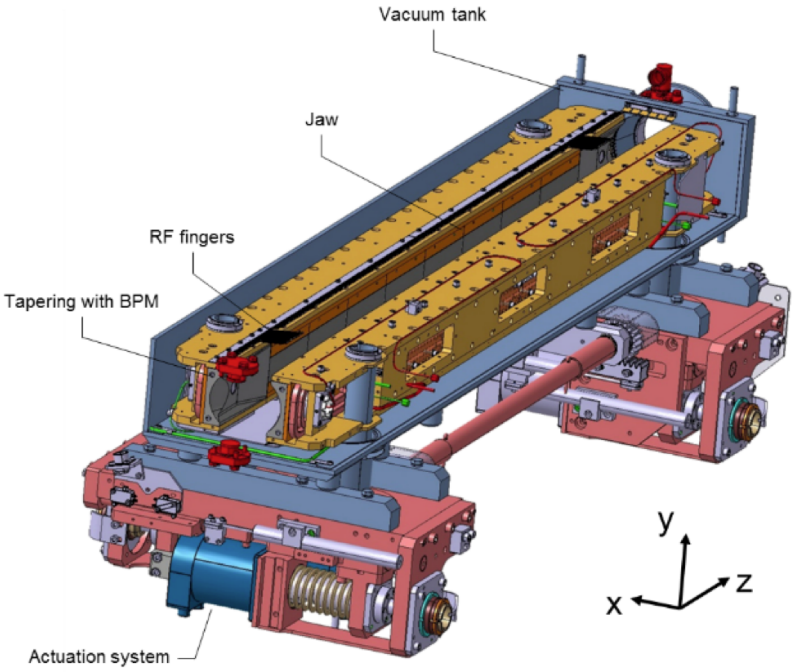

Figure 1: 3D drawing of the TCSPM collimator, showing an extremity of the jaw, with the embedded BPM, the “third” BPM for orbit measurements in the plane orthogonal to the collimation plane, and the new tapered transitions made of MoGr.

2 Present layouts and installation constraints

The layouts of the betatron and off–momentum collimation cleaning insertions were prepared for a low–impedance upgrade from the initial design phase [1]. Each TCSG secondary collimator of IR7 (22 devices) and IR3 (8), has an adjacent

slot called "TCSM", where "M" stands for *metallic*[1] [1]. An example taken from the 3D integration drawings of the machine is shown in Fig. 2. These slots are all equipped with the required cabling and ancillaries (support, cooling water, beam loss monitor, etc...) for the installation of a new collimator[2].

The installation of the new collimators can therefore be made either by replacing the existing TCSG collimators or by using the empty slots immediately downstream. The final decision for LS2 is to install the new collimators in the TCSM slots unless these are taken by prototypes or test devices installed in the LHC [5, 6] for MD activities; in this way, a hybrid scenario where both old and new collimators are temporarily kept operational could also be envisaged for Run III. This solution is not favoured for the long term because it would entail the maintenance of twice the number of devices, but could be considered as a temporary strategy for the initial commissioning of new collimators; the impact on the requirements for the collimator control units should also be assessed. Moreover, setting the TCSGs in the slots upstream of those of the new TCSPMs to parking position for LHC operations would be fine from the impedance point of view only in case of absence of non-conformities (e.g. from RF fingers, etc...) [7], which otherwise could make the impedance contribution of those collimators non-negligible, despite their open settings. Hence, after acquiring suitable experience with the new hardware in Run III, it could be envisaged to remove the IR7 TCSGs to avoid any possible impact on impedance from unused hardware.

It is also important to note that some of the TCSM slots and/or cabling were used in Run II for other test devices installed in IR7:

- the B2 slot TCSM.D4R7.B2 was used in 2017 for the installation of a low–impedance TCSPM prototype [5]; its layout name is TCSPM.D4R7.B2;
- the symmetric slot for B1 was used in 2015 for the installation of a crystal collimator device [6];
- three other sets of cables for TCSM slots were used in 2015 and 2017 for crystal collimator devices [6, 8].

These constraints will have to be taken into account for the assessment of LS2 activities. The test devices will remain at their place; hence, the TCSGs presently in the IR7 slots D4 will be replaced by the new TCSPMs.

[1] The new collimator name adds a "P" indicating the presence of orbit pick–ups.

[2] It is noted that cabling for the readout of the beam position monitors integrated in the jaw were not part of the initial installation because the previous design did not include this design feature. The short, radiation–hard cables from the tunnel's cable trays to the collimator support are also not installed for every TCSM slot.

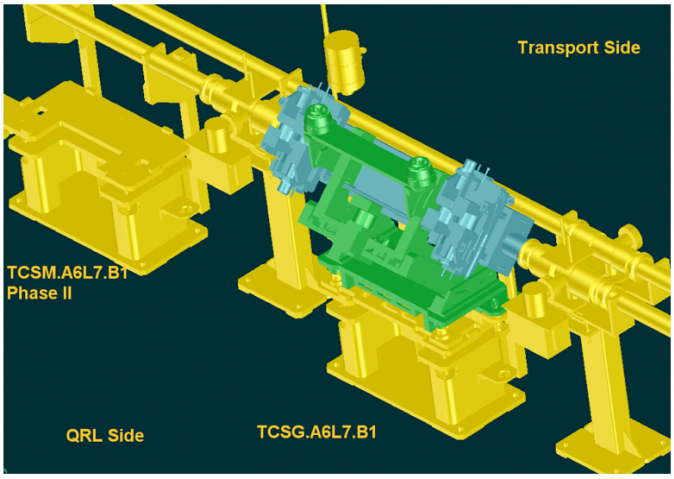

Figure 2: 3D integration drawing of a secondary collimator slot in IR7, showing the present TCSG collimator and the adjacent "TCSM" empty slot for future upgrade of the system. Both slots were fully cabled in the initial installation phase of the collimation system. 22 empty slots are available in IR7 and 8 in IR3.

3 Highlights of TCSPM design

The design of the new collimators (see Fig. 1) relies on a modular concept that allows embarking different absorber materials in the jaws, with no other impact or modifications to the other collimator components. The design can thus be adopted indifferently for primary, secondary and tertiary collimators, with obvious advantages for the series production. A detail of the jaw design is shown in Fig. 3. The "third BPM" for orbit measurements in the plane orthogonal to the collimator jaw movement is also visible. It measures the orbit position in the plane transverse to that of the jaw movement.

According to the present baseline, the TCSPM collimator jaws are made of MoGr [9], while tertiary collimators for HL–LHC will be built with Copper–Diamond (CuCD) jaws [10], which increases the robustness of the absorber against particle beam impacts with respect to the tungsten alloy adopted so far. A 5 to 6 μm–thick Molybdenum coating will be applied to the MoGr blocks to reduce further the TCSPM electrical resistivity, optimizing the behaviour of the component in terms of RF impedance. The coating cannot be applied to a primary collimator, as the thermal loads in operation are mostly concentrated on a thin material layer at the jaw beam face [11]. Four primary collimators will be built in MoGr and be installed in LS2 together with the new TCSPMs.

In the case of a secondary collimator (TCSPM) the active jaw length is 100 cm and the absorber is made of eight blocks, each 125 mm long. It is interesting to

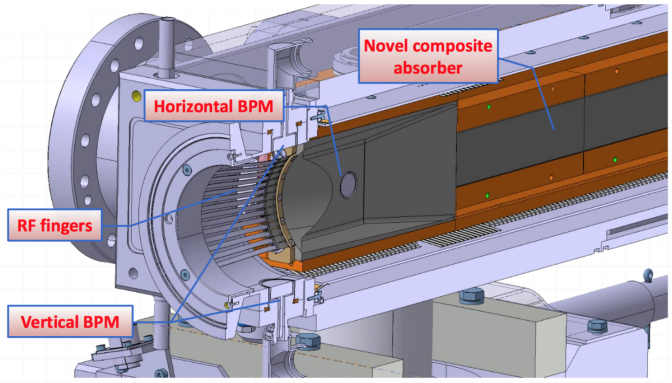

Figure 3: 3D drawing of the TCSPM collimator, showing an extremity of the jaw, with the embedded BPM, the "third" BPM for orbit measurements in the plane orthogonal to the collimation plane, and the new tapered transitions made of MoGr.

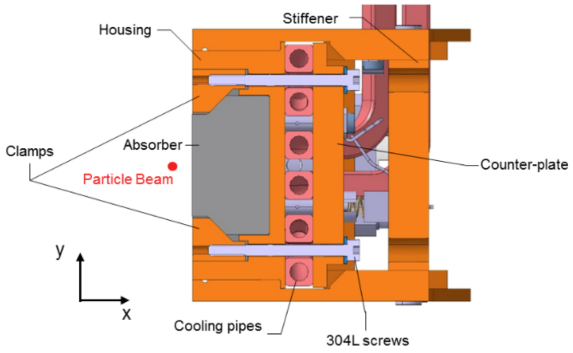

Figure 4: Transverse cross section of the TCSPM jaw at the mid location, where the active material is 25 mm thick.

note that the active jaw length of the primary collimator (TCPPM) is 60 cm. This shorter length is achieved by decreasing the MoGr blocks' thickness from 125 mm to 120 mm, through two transition regions on the second and on the last but one blocks of the jaw. A transverse cross section of the new jaw, at a central location with the full block thickness of 25mm, is given in Fig. 4.

A summary of the thermo–physical properties of MoGr is reported in Table 1. For reference, we also report the same properties for CuCD that is considered for future tertiary collimators. While CuCD is an isotropic material, MoGr is transversely isotropic, and this is due to its production process[3].

[3]In fact, the graphitic matrix is compressed at temperatures above the melting point of the molybdenum carbides created during the cycle; the liquid phase acts as a catalyst for the graphitization of the structure, with the creation of graphite planes with very good properties in the direc-

Table 1: Main thermo–physical properties of the MoGr used for the TCSPM collimator, and of the CuCD composite that is being considered for future upgrade of the LHC tertiary collimators.

Property	Direction	MoGr	CuCD
Density (g cm^{-3})	–	2.50	5.25
Thermal diffusivity (mm^2 s^{-1})	x	31.4	189.2
	y	468.9	189.2
	z	468.9	189.2
Specific heat (J kg^{-1} K^{-1})	–	601	340
Thermal conductivity (W m^{-1} K^{-1})	x	47.2	337.9
	y	706.2	337.9
	z	706.2	337.9
Thermal expansion coefficient	x	11.70	6.56
(μm m^{-1} K^{-1})	y	1.33	6.56
	z	1.33	6.56
Young's modulus (GPa)	x	4.7	160.0
	y	76.7	160.0
	z	76.7	160.0
Shear's modulus (GPa)	xy	3.8	75
	yz	33.0	75
	zx	3.8	75
Poisson's ratio	xy	0.10	0.07
	yz	0.16	0.07
	zx	0.10	0.07
Flexural strength (MPa)	x	11.5	104
	y	80	104
	z	80	104
Flexural strain to failure (μm m^{-1})	x	5140	5750
	y	1960	5750
	z	1960	5750

With the new design, the taperings are also upgraded from the TCSG design, and are made of MoGr instead of Glidcop. Numerical analyses and recent tests at the HiRadMat facility, in fact, showed that Glidcop cannot sustain the accidental design scenario of beam injection errors, whilst no problems were found in the case of a MoGr tapering [12]. The signal of the three BPMs is extracted through coaxial cables, made of stainless steel, with a glass–ceramic junction at the level of the feed–throughs to ensure the UHV tightness. The configuration of the cables was optimized by means of numerical calculations to minimize the stresses induced on it during opening and closing of the two jaws.

The jaw design was performed with the goal of minimizing the temperature and the bending deformation induced by the beam losses in the nominal design scenario for steady beam losses. For this reason, the contact between the active jaw and the Glidcop housing was improved with respect to CFC collimators, with a contact pressure increased from 3 bar to 18 bar. Technically, the upgrade was possible thanks to a clamping system (see Fig. 4) with the contact force given by screws instead of the old springs. This significantly improves the thermal conductance at the contact interface, with a beneficial effect on the maximum temperature reached by the absorber blocks. Moreover, the housing and stiffener have a higher rigidity, increasing the moment of inertia of the section and reducing the deformations. Nevertheless, beam losses as high as at the HL–LHC, reaching the level of 1 MW, remain a challenge for collimators.

4 Comparative assessment of alternative layouts

4.1 General considerations

Various considerations have to be taken into account in the choice of optimum slots for new collimators. The first one is the assessment of single–collimator contributions to the total machine impedance. This is of primary importance for the specific scope of the LS2 upgrade that is aimed at minimizing the collimator impedance in Run III, given the constraint that only 4 new collimators per beam will be available.

On the other hand, other aspects of the operation at high intensity should not be underestimated for the choice of optimum layouts: (1) total beam loads, and corresponding thermo–mechanical response of the collimators, during standard and abnormal loss rate scenarios; (2) exposure of individual secondary collimators, and of their coated surface, to fast design failures at injection and at top energy; (3) impact on the collimation cleaning performance. Note in particular

tions parallel to the plane, and lower values of the property parameters in the direction orthogonal to the planes.

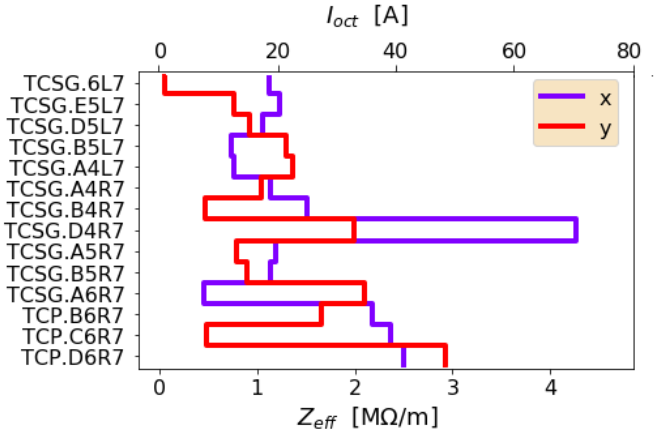

Figure 5: Computed single–collimator contribution to the dipolar impedance and the corresponding octupole current required to stabilize the beams. The imaginary part of the effective impedance is plotted for the ultimate operational scenario at the top energy of 7 TeV [13]. The octupole current contributions are estimated from a scaling of the dipolar impedance.

that the LIU upgrade is scheduled to be completed by LS2 and therefore higher intensity beams will progressively become available in Run III. Also note that the LS2 installation for the operation in Run III will likely remain untouched in LS3 for the final HL–LHC layouts and therefore the new slots equipped in LS2 should be considered as final for the HL–LHC era.

The dipolar impedance of individual IR7 TCSGs, as well as the corresponding current needed for stabilization through the Landau octupoles, are shown in Fig. 5. Since these collimators dominate the total impedance of the machine, the stabilizing octupole current is roughly proportional to their impedance contributions. It can be seen that, among the secondary collimators, the largest single contributors to the machine impedance are TCSG.D4R7.B2 in the horizontal plane and TCSG.A6R7.B2 in the vertical plane. The specular slots for B1 yield the same result.

The fast design failures that we consider are injection failure, at injection energy and injection optics (in the vertical plane), and extraction failure (asynchronous beam dump) at top energy (in the horizontal plane). To quantify the risk of impacting a certain collimator during beam failures, we show in Tables 2–3 the phase advances from the injection and extraction kickers in the respective planes. For injection failure, we consider the injection optics, while for asynchronous beam dump we consider the optics at the end of ramp and squeeze, as well as the end point of the squeeze, for each configuration. As the optics in Run III is not yet known, we study optics for both HL–LHC v1.3 and the 2017 ATS optics.

The closer the fractional phase advance is to 90° or 270°, the larger is the excursion of the oscillating trajectory caused by a mis–fired kicker. Hence, the collimators with such phase advances are the most critical in terms of robustness. As it can be seen, the TCSG.D4L7.B1, which is the only purely vertical TCSG and also has the highest impedance contribution, has a vertical phase advance from the injection kicker close to 90° for HL–LHC v1.3. Furthermore, the TCSG.B4L7.B1 has a horizontal phase advance from the dump kicker which is close to 270° in both HL–LHC v1.3 and the 2017 ATS optics, and TCSG.6R7.B2 is close to 90°. We consider these collimators as being the most likely to be hit by beam during the design failures.

In spite of these phase advances, the risk of damage is still very small. The robustness in case of injection failure has been tested in HiRadMat [14], where 288 bunches of 1.4×10^{11} protons per bunch impacted a MoGr TCSPM collimator with Mo coating. This did not result in any plastic damage of the jaw, but only in a small scratch in the coating. A fresh surface could be recovered by moving the collimator along the 5^{th} axis. Even though the used bunch population is around 60% of the one foreseen for HL–LHC, it is extremely pessimistic that such a large fraction of the full beam would hit a TCSPM. Tracking simulations show that, even in the presence of pessimistic imperfections at the injection protection [15], the escaping protons reaching any single TCSG in IR7 during an injection failure is smaller.

The case of asynchronous dump is less critical than injection failure for the collimator robustness. Simulations using the setup described in Ref. [16] of a single–module type 2 pre–fire, which is the most critical known failure mode of the extraction kickers, indicate that up to around 7×10^{11} protons could be expected to impact the most exposed secondary collimators, if 2.2×10^{11} protons per bunch are assumed as normalization factor. This impact is still significantly less critical than the injection failure, and a linear scaling of the stress from this case gives about a factor 10 safety margin to the threshold where plastic deformation occurs. Still, a local peal–off of the Mo coating cannot be excluded, in which case a fresh surface could again be recovered by use of the 5^{th} axis.

In conclusion, for all considered failure modes, there is no risk of damage of the collimator except that the coating could be scratched; anyway, in such cases, the collimator can be moved remotely to expose an undamaged surface to the beam without any impact on operation. Such a recovery action cannot be done too many times, but since this type of severe accident is very rare, the risk is considered acceptable.

Table 2: The horizontal fractional phase advance ($\Delta\mu_x$) in optics version HL–LHC v1.3, as of January 2018, from the dump kickers in each beam, MKD.O5L6.B1 or MKD.O5R6.B2, and the vertical fractional phase advance ($\Delta\mu_y$) from the injection kickers, MKI.C5L2.B1 or MKI.C5R8.B2, to each of the TCSGs in IR7, for different values of β^*. We show also the transverse angle of the collimation plane (0 degrees corresponds to a horizontal collimator, 90 degrees to a vertical collimator).

Collimator	Angle (deg)	$\Delta\mu_x$ (deg) β^* =15 cm	$\Delta\mu_x$ (deg) β^* =64 cm	$\Delta\mu_y$ (deg) β^* =6 m
TCSG.A6L7.B1	141.0	185.0	180.0	68.8
TCSG.B5L7.B1	144.0	261.0	256.0	81.6
TCSG.A5L7.B1	40.7	262.0	257.0	83.1
TCSG.D4L7.B1	90.0	267.0	262.0	96.0
TCSG.B4L7.B1	0.0	283.0	278.0	152.0
TCSG.A4L7.B1	135.0	285.0	280.0	153.0
TCSG.A4R7.B1	46.3	287.0	282.0	155.0
TCSG.B5R7.B1	141.0	8.0	3.3	174.0
TCSG.D5R7.B1	51.4	13.7	8.9	179.0
TCSG.E5R7.B1	130.0	14.7	9.9	180.0
TCSG.6R7.B1	0.5	20.7	16.0	210.0
TCSG.A6R7.B2	141.0	224.0	233.0	345.0
TCSG.B5R7.B2	144.0	299.0	309.0	357.0
TCSG.A5R7.B2	40.6	300.0	310.0	359.0
TCSG.D4R7.B2	90.0	305.0	315.0	11.4
TCSG.B4R7.B2	0.0	320.0	330.0	65.7
TCSG.A4R7.B2	132.0	322.0	331.0	67.5
TCSG.A4L7.B2	42.1	330.0	339.0	73.6
TCSG.B5L7.B2	141.0	46.8	56.4	90.2
TCSG.D5L7.B2	51.4	52.5	62.1	94.6
TCSG.E5L7.B2	130.0	53.5	63.1	96.1
TCSG.6L7.B2	0.5	59.5	69.2	125.0

Table 3: The horizontal fractional phase advance ($\Delta\mu_x$) in the 2017 ATS optics from the dump kickers in each beam, MKD.O5L6.B1 or MKD.O5R6.B2, and the vertical fractional phase advance ($\Delta\mu_y$) from the injection kickers, MKI.C5L2.B1 or MKI.C5R8.B2, to each of the TCSGs in IR7, for different values of β^*. We show also the transverse angle of the collimation plane (0 degrees corresponds to a horizontal collimator, 90 degrees to a vertical collimator).

Collimator	Angle (deg)	$\Delta\mu_x$ (deg) β^* =30 cm	$\Delta\mu_x$ (deg) β^* =1 m	$\Delta\mu_y$ (deg) β^* =11 m
TCSG.A6L7.B1	141.0	190.0	186.0	354.0
TCSG.B5L7.B1	144.0	265.0	261.0	7.0
TCSG.A5L7.B1	40.7	266.0	263.0	8.5
TCSG.D4L7.B1	90.0	271.0	267.0	21.4
TCSG.B4L7.B1	0.0	288.0	284.0	77.1
TCSG.A4L7.B1	135.0	289.0	286.0	78.8
TCSG.A4R7.B1	46.3	291.0	288.0	80.4
TCSG.B5R7.B1	141.0	12.5	8.9	99.6
TCSG.D5R7.B1	51.4	18.0	14.5	104.0
TCSG.E5R7.B1	130.0	19.0	15.5	106.0
TCSG.6R7.B1	0.5	25.0	21.5	136.0
TCSG.A6R7.B2	141.0	240.0	239.0	36.3
TCSG.B5R7.B2	144.0	316.0	316.0	49.0
TCSG.A5R7.B2	40.6	318.0	317.0	50.4
TCSG.D4R7.B2	90.0	322.0	322.0	62.9
TCSG.B4R7.B2	0.0	337.0	337.0	117.0
TCSG.A4R7.B2	132.0	339.0	338.0	119.0
TCSG.A4L7.B2	42.1	347.0	346.0	125.0
TCSG.B5L7.B2	141.0	63.7	63.0	142.0
TCSG.D5L7.B2	51.4	69.5	68.8	146.0
TCSG.E5L7.B2	130.0	70.5	69.9	148.0
TCSG.6L7.B2	0.5	76.6	75.9	177.0

4.2 Considered layout configurations

Taking into account the constraints above, four different configurations were considered for detailed impedance, cleaning and robustness calculations. The rationale for these choices is summarized below. The list of collimators considered for the upgrade, with the detailed layout information for all the IR7 collimators, is given in Table 4 for Beam 1 (Beam 2 layouts are equivalent and symmetric around IP7 [1]). In all cases, we start from the list of the single collimator contributions to the impedance, see Fig. 5, and we assume that the units with largest contributions are replaced first (called configuration C–1). This would be the obvious choice if impedance reduction was the only constraint. According to the impedance simulations (Fig. 5), the secondary collimator with the highest contribution to the horizontal dipolar impedance and the corresponding octupole current is the D4R7, and to the vertical – the A6R7. Alternative configurations are elaborated by assuming that some of the highest contributors to impedance shall not be addressed for other motivations:

C–1 replacement of the collimators with the largest single contributions to machine impedance without taking into account any other constraints from loss scenarios;

C–2 exclude the replacement of the first two skew collimators downstream of the primary collimators that are the most exposed to regular collimation losses in terms of energy deposition;

C–3 exclude collimators in the horizontal and vertical planes that are effected by failure cases at injection and at top energy (asynchronous dump);

C–4 exclude only horizontal secondary collimators that are affected by the top energy failure, and not the vertical one affected by injection failures only.

4.3 Impedance contributions

The LHC impedance at the top energy is driven by the resistive wall contribution of its collimation system [17]. For the current Hi–Lumi OP scenario [13] the total octupole threshold with CFC collimators is about 400 A, close to the limit of the octupole current (Fig. 6). Nearly all of the octupole threshold is created by the collimation system, and almost a half comes from the secondary collimators in IR7. The second largest contributors are the four primary collimators, responsible for about a quarter of the octupole threshold.

The full upgrade of all TCSGs in IR7 will reduce their resistive wall impedance dramatically. The total impedance of the secondary collimators in IR7 will decrease by a factor of four for the latest HL–LHC operational scenario (Fig. 7).

Table 4: List of IR7 collimators: primary, TCP; secondary, TCSG; shower absorbers, TCLA. Their longitudinal position from IP1, s, and from IP7, s_{IR7}, horizontal and vertical betatron functions, β_x, β_y are listed; distances are taken from the end of the active length. The skew angles are reported as well (0: horizontal; 90: vertical; else: skew). The TCSG marked as '☑' are the ones that are replaced by the new TCSPM design in the different configurations C–1, C–2, C–3 and C–4 considered in the comparative assessment of alternative LS2 layouts. B1 layouts are considered. The symmetric configurations are considered for B2.

Name	s [m]	s_{IR7} [m]	β_x [m]	β_y [m]	Angle [deg]	Configuration 1	2	3	4
TCP.D6L7.B1	19789.5	-204.7	157.6	78.9	90				
TCP.C6L7.B1	19791.5	-202.7	149.3	83.5	0				
TCP.B6L7.B1	19793.5	-200.7	141.3	88.2	127.5				
TCSG.A6L7.B1	19833.2	-161.0	39.3	229.3	141.1	☑	☐	☑	☑
TCSG.B5L7.B1	19892.4	-101.8	163.1	163.9	143.5	☑	☐	☑	☑
TCSG.A5L7.B1	19896.4	-97.8	189.4	143.5	40.7	☐	☐	☑	☑
TCSG.D4L7.B1	19917.7	-76.4	335.0	68.0	90	☑	☑	☐	☑
TCSG.B4L7.B1	19987.7	-6.5	138.3	132.2	0	☑	☑	☐	☐
TCSG.A4L7.B1	19991.7	-2.5	127.3	142.6	134.6	☐	☐	☑	☐
TCSG.A4R7.B1	19995.7	1.5	117.0	153.6	46.3	☐	☐	☐	☐
TCSG.B5R7.B1	20086.9	92.8	124.3	263.7	141.5	☐	☐	☐	☐
TCSG.D5R7.B1	20102.9	108.8	217.2	155.6	51.4	☐	☐	☐	☐
TCSG.E5R7.B1	20106.9	112.8	245.0	133.4	130.5	☐	☑	☐	☐
TCSG.6R7.B1	20141.5	147.4	332.9	47.3	0.5	☐	☑	☐	☐
TCLA.A6R7.B1	20148.6	154.4	294.4	48.3	90				
TCLA.B6R7.B1	20179.5	185.3	157.7	77.2	0				
TCLA.C6R7.B1	20212.7	218.6	67.7	153.4	90				
TCLA.D6R7.B1	20214.7	220.6	64.2	159.5	0				
TCLA.A7R7.B1	20232.4	238.2	65.4	144.5	0				

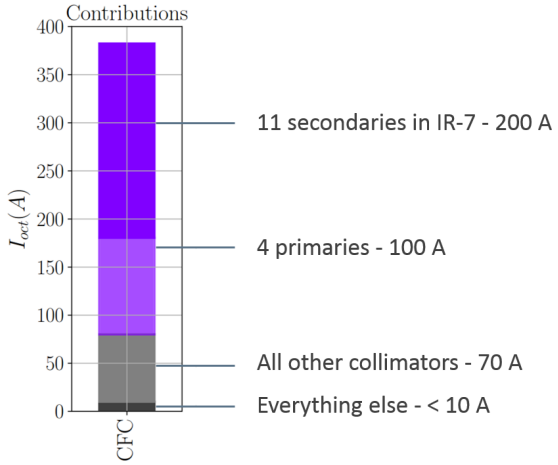

Figure 6: Different contribution to octupole current required by the present collimation system. The impedance of LHC collimators has to be reduced in order to ensure the coherent beam stability for HL–LHC. The octupole current in the most critical plane (i.e. the horizontal one) and the most relevant contributions at the top energy of 7 TeV for Ultimate OP scenario [13] are shown [18]. The maximum available stabilizing octupole current is 570 A. Reference simulation parameters: damper gain: $d = 100$ turn^{-1}; chromaticity: $Q' = 10$; normalised emittance: $\varepsilon_n = 2.0\ \mu$m.

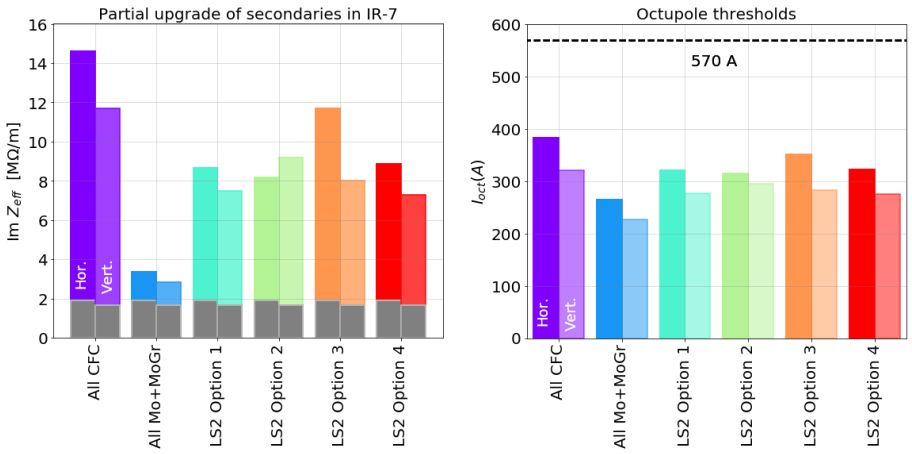

Figure 7: Impedance from IR7 TCSG collimators (left frame) and corresponding required octupole currents (right frame) for different layout configurations for the Ultimate OP scenario [13]. Options C–1, C–2, and C–4 offer similar reduction of the impedance of the secondaries in IR7. The second option seems slightly more preferable, since it provides a larger impedance reduction in the more critical horizontal plane. Colored bars show the resistive wall contributions of the IR7 secondaries for various coating scenarios in both transverse planes, and the gray ones show the geometric part of impedance.

A partial upgrade of the secondary collimators provides up to 50% of the total impedance reduction in IR7, depending on the chosen installation scenario. Apart from the third upgrade scenario, all options offer a similar reduction of the total machine impedance, with the second one being slightly preferable from the impedance point of view. The reason is that the second option offers the largest reduction in the horizontal plane, which is the most critical for the coherent beam stability: due to the impact of other sources of impedance the horizontal impedance is larger than the vertical one, requiring a greater octupole current to stabilize the beam. Since the octupole threshold is the maximum of the two, horizontal and vertical, it is beneficial to maximize the impedance reduction in the horizontal plane. That is achieved with the option C–2. The C–1 option, although it includes the highest contributing collimators in both planes, leads to a slightly lower impedance reduction in the horizontal plane and, as a consequence, a slightly higher octupole threshold.

Figure 8 depicts individual collimator contributions to the resistive wall (RW) (left) and geometric (right) parts of effective imaginary dipolar impedance for the current baseline. The RW contribution comes mainly from three sources: the primary collimators (TCPs), the secondary collimators (TCSGs) in IR7, and TCSGs

in IR3. These last ones, not upgraded in the baseline, show an extra potential for impedance reduction. Their upgrade would further reduce the machine impedance in the vertical plane. Contrary to the RW part, there are no dominant contributors to the geometric part (Fig. 8, right). This may be explained, in part, by the approximation of the model used in the present study that does not distinguish the tapers of different types of collimators and assumes a flat–taper geometry. As the RW part of impedance is reduced thanks to the low–impedance coatings, it becomes important to accurately model the geometric component. More refined studies dedicated to the estimation of the geometric impedance of all types of secondary collimators [19] showed that the overall impact of the detail of the taper geometry on the machine impedance is 1 % in the case of LHC and below 3 % in the case of HL-LHC; in the near future, the LHC impedance model will be refined to account for the difference in taper geometries.

4.4 Beam loss simulations

For each considered configuration (see Sec. 4.2), cleaning simulations were performed in order to quantify the local cleaning inefficiency in the regions of the dispersion suppressor (DS) downstream of the betatron collimation system in IR7. The local cleaning inefficiency maps the leakage by the collimation system all along the LHC ring; its maximum at cold elements is generally found in the DS immediately downstream of IR7 [20]. The simulations were carried out with the SixTrack–FLUKA coupling [21]. These simulations also allow one to generate a suitable input to energy deposition studies, which in turn can be used for further thermo–mechanical analyses.

The simulations were carried out using the thin–lens version of the HL–LHC optics v1.3 [22]. Two working points were simulated:

- β^* =6 m: in this configuration, a TCLD collimator in cell 8 downstream of IR7 is taken into account; moreover, a special version of the IR7 optics [23] was deployed, re–matched for the removal of the MQWA.E5[L,R]7;
- β^* =15 cm: in this configuration, no TCLD collimator is considered in the LHC sequence.

The first scenario corresponds to the HL–LHC configuration at the end of the ramp as planned at the time of writing. The second scenario corresponds to the smallest β^* optics foreseen for HL–LHC and the choice of not using TCLD collimators represents a conservative case for the loads on the tertiary collimators around the high–luminosity points. Table 5 summarises the collimator settings used in simulation. Note that the local cleaning inefficiency, which is the focus of the following, does not depend significantly on the optics choices in the experimental insertions. This is because those losses are dominated by protons scattered

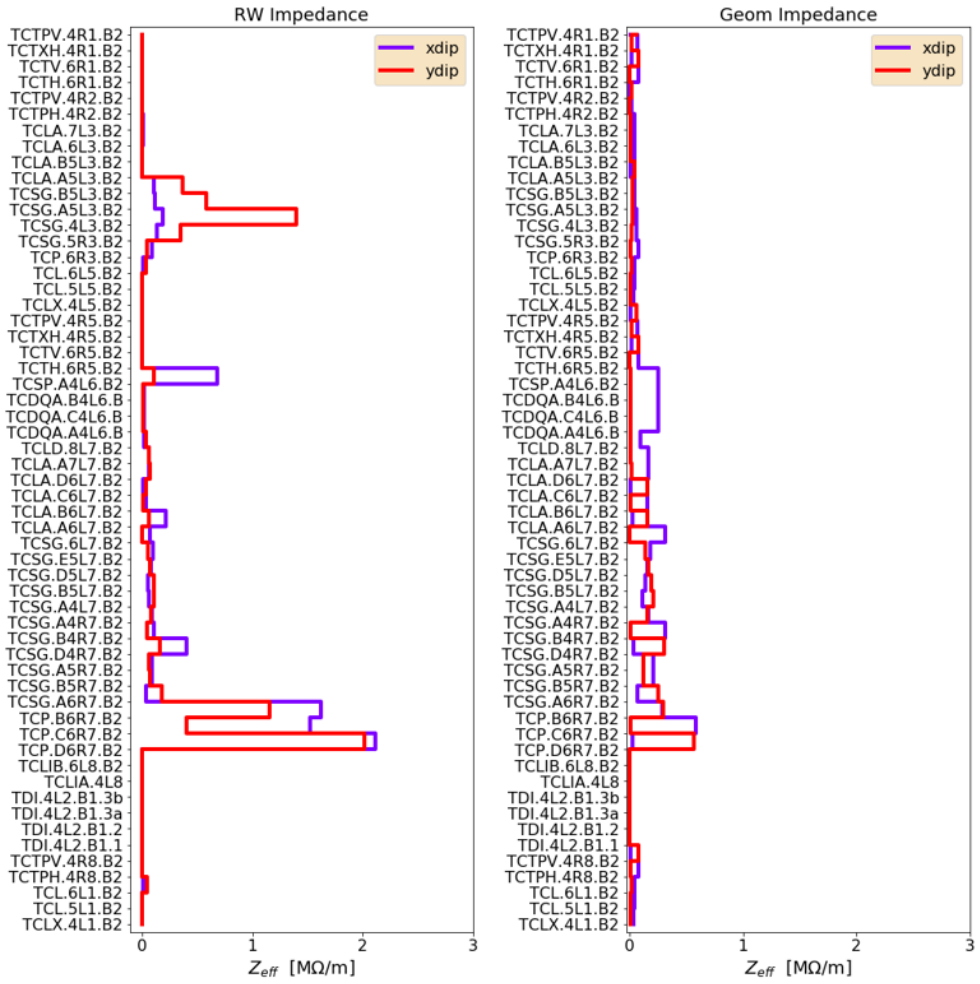

Figure 8: Distribution of collimator impedance after all the secondaries in IR7 are upgraded. The resistive wall impedance (left frame) can be further reduced by coating the secondaries in IR3, but is mainly determined by the TCPs in IR7. There are no dominant contributors for the geometric part (right frame). The imaginary part of Z is plotted for a chromaticity $Q' = 0$.

Table 5: Collimator settings used in the simulations at β^* =6 m, where a TCLD installed in cell 8 and the removal of MQWA.E5[L,R]7 were taken into account, and at β^* =15 cm, where no TCLD in the LHC lattice structure was considered.

IR	Coll Families	β^* [m]	ε = 2.5 μm [σ]	ε = 3.5 μm [σ]
3	TCP/TCS/TCLA		17.7/21.3/23.7	15/18/20
7	TCP/TCS/TCLA/TCLD	6	6.7/9.1/12.7/16.6	5.7/7.7/10.7/14
		0.15	6.7/9.1/12.7/out	5.7/7.7/10.7/out
6	TCDQ/TCSP	6	12.3/12.3	10.4/10.4
		0.15	10.1/10.1	8.5/8.5
1/5	TCT/TCL	6	43.8/out	37/out
		0.15	10.4/14.2	8.8/12
2	TCT	6	43.8	37
		0.15	43.8	37
8	TCT	6	43.8	37
		0.15	17.7	15

out of the primary collimators with a sufficiently high value of $\delta = \Delta p/p$ that are lost at the first dispersion peaks [20]. For the same reason, it is expected that the change of absorbing material of the jaw of secondary collimators does not worsen the local cleaning inefficiency in the IR7 DSs substantially, especially if the new material has average atomic number and density slightly higher than those of the material presently deployed, since the cross sections increase.

The tracked beam was sampled with transverse distributions standard to cleaning simulations, i.e. flat on the cleaning plane and Gaussian on the non–cleaned plane, in the range ± 3 σ [24]. A full thickness of 0.04 σ was chosen on the cleaning plane, resulting in an average impact parameter of *e.g.* $\sim$4 μm on the horizontal plane[4], in order to have a fairly superficial impact but not too thin, relevant for the losses in the DS. The beam was monochromatic in energy, since protons lost in the DS have values of δ way larger than the initial one of the beam, due to scattering events in the collimator jaws; hence, no longitudinal distribution was considered. The beam was sampled at the collimator, considering only those protons in direct view of the jaws ("pencil beam"). In this way, losses are balanced between the two jaws of the primary collimator directly impacted; this implies also a slightly better use of the CPU time.

Figure 9 shows a comparison of the B1H loss maps (i.e. when losses take

[4]For the vertical plane, a similar figure cannot be given, as the beam is defocussed, and protons impact the jaw on the faces in view of the beam; hence proton impacts are diluted over the jaw, averaging at 2/3 of the active length.

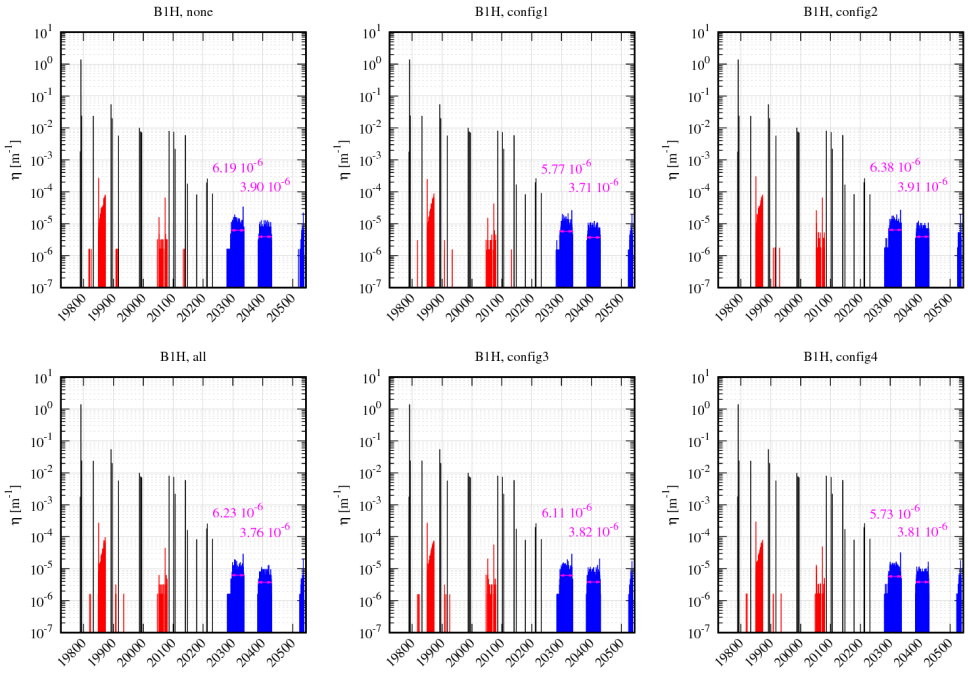

Figure 9: B1H loss maps simulated with the SixTrack–Fluka coupling; the zoom on IR7 and the downstream DS is shown. The case of β^* =15cm is shown, without TCLDs.

Table 6: Average cleaning inefficiencies in the DS downstream of IR7 as predicted by SixTrack–Fluka coupled simulations for the various combinations of TCSPM slots. The case of no TCSPM installed ("None") and of the post–LS3 era (i.e. with all TCSPM installed) are shown as well, for reference. Simulations at β^* =15 cm take into account no TCLD installation; hence, values refer to the first cluster of DS losses. Simulations at β^* =6 m take into account both TCLD installed in cell 8 and removal of MQWA.E5[L,R]7; hence, values refer to the second cluster of DS losses, since the first cluster is substantially reduced by the upstream TCLD.

Simulated Scenario	None [10^{-6}]	C–1 [10^{-6}]	C–2 [10^{-6}]	C–3 [10^{-6}]	C–4 [10^{-6}]	post–LS3 [10^{-6}]
β^* =15 cm, B1H	6.19	5.77	6.38	6.11	5.73	6.23
β^* =15 cm, B1V	5.33	5.12	5.17	5.32	5.07	5.34
β^* =6 m, B1H	2.47	2.41	2.45	2.34	2.35	2.25
β^* =6 m, B1V	3.73	3.52	3.55	3.70	3.58	3.84

place on B1 on the horizontal plane) expected for the four considered configurations, zoomed on the region of IR7 and the downstream DS. The case of no change at all ("None") and with all IR7 TCSG exchanged ("All", corresponding to the post–LS3 configuration) are shown as well, for comparison. Both the two classical IR7 DS clusters are visible, since the simulated configuration does not consider TCLDs; the average cleaning inefficiency along the clusters are reported in the figure as well. As it can be seen, the loss maps are perturbed but with no substantial difference. The same conclusion can be drawn from B1V loss maps, and for β^* =6 m. The complete set of average cleaning inefficiencies is summarized in Tab. 6. For each simulated scenario, all the configurations agree within ± 5 %; hence, they can all be considered equivalent.

4.5 Thermo–mechanical response to steady beam losses

An example of typical beam load in W at each TCSG is given in Fig. 10, detailing loads on both jaws separately and the total for the two jaws together. They are calculated with a complex simulation setup that starts from the multi–turn cleaning simulations of halo particles [25] and then uses energy deposition tools to assess losses in the whole IR7 [26]. This is a time– and resource–consuming setup that cannot be realistically done for all the configurations considered here. We consider instead the configuration of the proton collimation quench test done in 2015 [27] for beam 2 that was studied in detail. This is considered sufficient to evaluate reliably the relative loss balance between the different TCSG collimators,

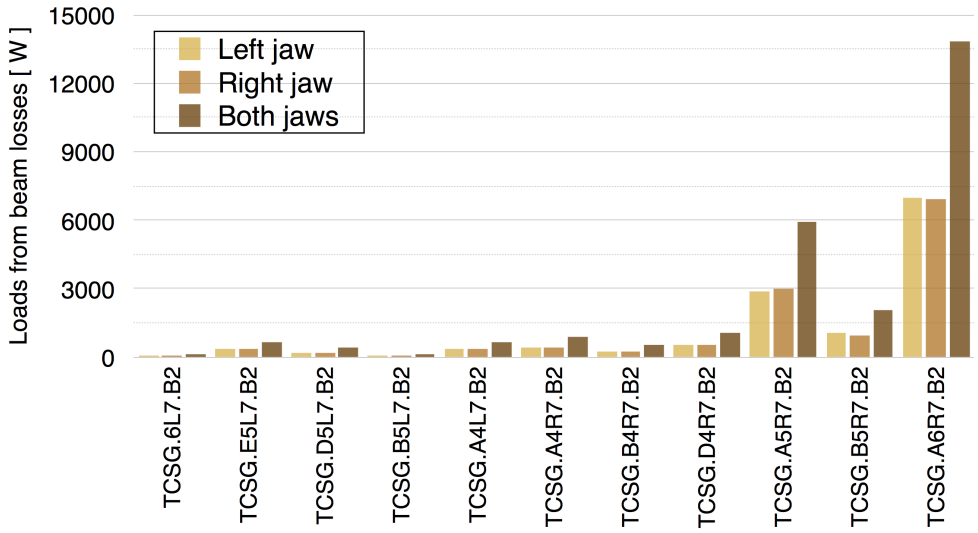

Figure 10: Beam loads on the secondary collimators for horizontal primary losses of 500 kW, for the beam 2 case studied in 2015 during the proton collimation quench test.

while we plan a final assessment to be finalized for the baseline proposed solution. It is seen that, for this horizontal loss scenario, the first skew collimator takes about 50 % of the total losses absorbed by the secondary collimators (13.8 kW for a total of 26.3 kW). The relative losses, normalized by the total power absorbed in all TCSGs, is shown for completeness in Fig. 11.

The thermo–mechanical response of the jaw has to be verified against the design scenarios of slow losses from the circulating particle beam. In particular, a numerical steady–state analysis is performed with the load on the collimation system equivalent to 1 h beam lifetime (BLT). This corresponds to total losses of 1.68×10^{11} protons/s (*i.e.* 200 kW of primary beam losses). A second analysis relevant for the collimator design foresees losses equivalent to 0.2 h BLT lasting for 10 s, for a total peak load of about 1 MW on the system. In this case, the numerical simulation performed is a transient one.

As seen above, the most loaded collimator is the first skew one, *i.e.* the TCSG.A6L1.B1, and the losses on this component are assumed as the reference case for the design of the TCSPM. The load on the collimator is 20 kW in the 1 h BLT case, and 100 kW for 0.2 h. The temperatures achieved in this second, more demanding scenario, are shown in Fig. 12. A breakdown of the loads on the jaw for different absorber materials, as well as a comparison with the LHC load on a standard TCSPM, is shown in Tables 7 and 8 for the two considered beam loss cases.

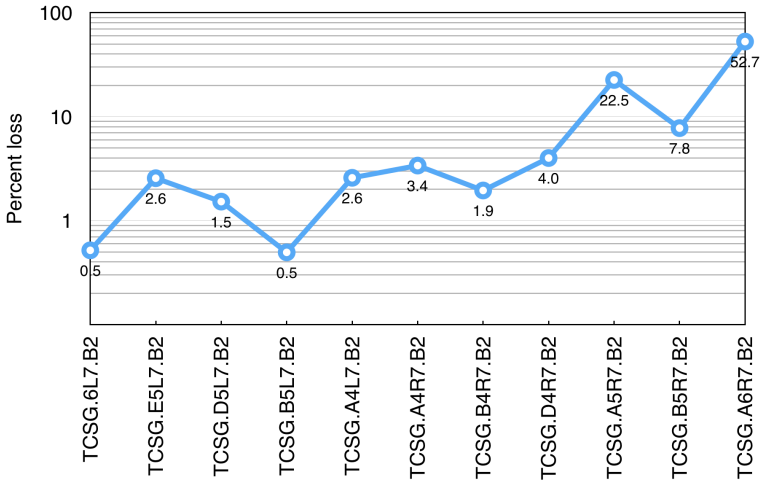

Figure 11: Relative distribution of loads to the present LHC secondary collimators for the 2015 proton collimation quench test loss scenario described in the text (peak loss of 500 kW). Single collimator losses of Fig. 10 are normalized by the total loss on all secondaries.

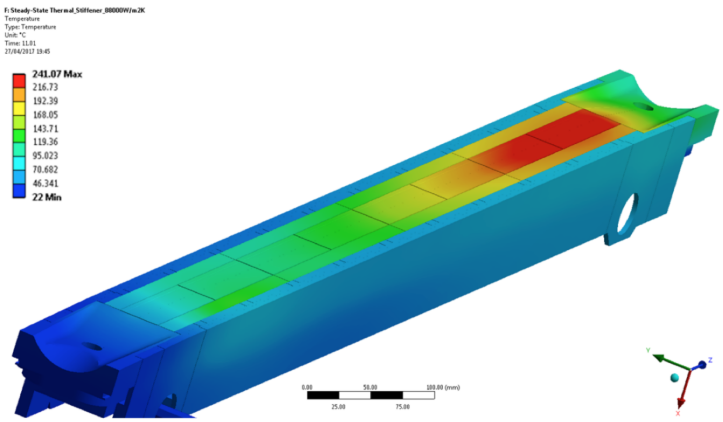

Figure 12: Temperature profile on the TCSPM jaw in the 0.2h BLT scenario

Table 7: Energy deposition and beam–induced sagitta on a standard TCSG and on the new TCSPMs made of CFC or MoGr, for the LHC and HL–LHC beams in the 1 h beam lifetime case.

	1 h beam lifetime		
	$TCSG_{CFC}$ (LHC)	$TCSPM_{CFC}$ (HL–LHC)	$TCSPM_{MoGr}$ (HL–LHC)
Total energy on collimator (kW)	4.5	12.6	20.7
Energy on most loaded jaw (kW)	2	5.5	9.4
Energy on the absorber blocks (kW)	0.4	1.5	4
Total jaw deformation (μm)	83	110	76

Table 8: Energy deposition and beam–induced sagitta on a standard TCSG and on the new TCSPMs made of CFC or MoGr, for the LHC and HL–LHC beams in the 0.2 h beam lifetime case.

	0.2 h beam lifetime		
	$TCSG_{CFC}$ (LHC)	$TCSPM_{CFC}$ (HL–LHC)	$TCSPM_{MoGr}$ (HL–LHC)
Total energy on collimator (kW)	22.5	63	103.5
Energy on most loaded jaw (kW)	10	27.5	46.9
Energy on the absorber blocks (kW)	2	7.5	20
Total jaw deformation (μm)	96	300	505

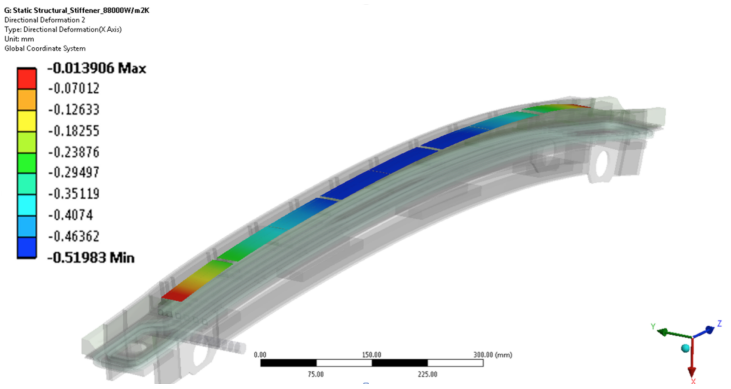

Figure 13: Bending deformation on the TCSPM jaw in the 0.2h BLT scenario, in mm. Note that the deformation is elastic, and the structure returns to the undeformed configuration when the load is removed

In terms of thermally induced stresses on the jaw elements, no problems are highlighted: the jaw is free to expand longitudinally, and the equivalent stress in operation is negligible. On the other hand, a stringent requirement is to limit the flatness error of the active surface to a maximum of 100 μm. This includes the machining tolerances, the deformation due to the self–weight and the beam–induced sagitta. While in the 1 h BLT case the total of these contributions is within the specification, in the 0.2 h BLT scenario the beam–induced sagitta is dominant, and above the requirements in the case of the skew collimator TCSG.A6L1.B1 (Fig. 13). As shown in Table 8, a large sagitta occurs also when CFC is adopted as absorber material, even though in that case the absolute value is 40 % lower[5].

5 Proposed baseline solution

Based on the considerations above, we propose to take the configuration C–2, *i.e.* the collimator slots:

- TCSG.D4L7.B1 / TCSG.D4R7.B2;
- TCSM.B4L7.B1 / TCSM.B4R7.B2;
- TCSM.E5R7.B1 / TCSM.E5L7.B2;
- TCSM.6R7.B1 / TCSM.6L7.B2.

[5]It can be seen that, for this specific case, the ratio of induced deformation in the 0.2h BLT scales almost linearly with the load on the jaw. As a very rough approximation, this observation could be extended also to the other collimators, even though significant deviations could take place in case of different load distributions on the jaw. For a more precise assessment, further simulations should be performed.

The TCSM slots are preferred over the TCSG ones immediately upstream, to give the possibility in Run III to run with a hybrid IR7 configuration where both new TCSPM and existing TCSG collimators are deployed to get acquainted to the new hardware; the new hardware is installed in the TCSG slots only in case the respective TCSM slot is already taken by test devices (see Sec. 2). Taking note that from the impedance point of view this solution is very close to the optimum solution C–1, the choice is primarily motivated by the observations on jaw deformation at peak loss rates presented in the previous section. While this is not expected to pose immediate limitations in Run III when it will not be possible to profit from the full LIU beams foreseen for HL–LHC, not equipping the most exposed secondary collimators allows further iterations on the TCSPM design to improve further the elastic deformation for the second stage of installation in LS3.

6 Conclusions

The choice of 8 secondary collimators that will be replaced in LS2 with the low–impedance design TCSPM was presented. The driving criterion for the proposed layout is the optimization of the impedance reduction of the IR7 collimation system, which in Run III will dominate the LHC machine impedance. Four different configurations were studied in detail in a comparative assessment that, in addition to the impedance improvements, also looked at the various aspects relevant for the Run III operation.

It was found that the impedance reduction that one would obtain with these configurations is comparable and amounts to a reduction of about 40 % of the present secondary collimator impedance. The cleaning performance in terms of dispersion suppressor losses is also equivalent, and essentially identical if one considers the Run III layout with new DS collimators TCLD around IR7. In these conditions, a driving term for the final layout choice is the observation that the new collimators absorb more efficiently products that emerge from the primary collimators because of the higher effective Z. This leads to dynamic deformations that, for the pessimistic design losses of 0.2 h beam lifetime, would induce a deformation close to 500 μm if the first skew secondary collimators were replaced. Note that in this case, also the present collimator would experience a transient deformation of 300 μm that is well above the system specification of 100 μm. Moreover, it should be noted that such deformation is an elastic one (hence with no permanent damage induced in jaw) and a temporary one, as it takes place at the peak in time of energy deposition, *i.e.* at the end of the load time of 10 s.

Such a large jaw elastic deformation would only be achieved if the total intensities planned for HL–LHC were achieved in Run III, which is extremely unlikely. Nevertheless, we consider as a prudent approach the choice to keep the first

two skew secondary collimators as they are now and replace collimators further downstream where loads are much reduced. This scenario ensures the possibility to operate safely in Run III while testing the new collimator design, and leaves time to improve further the TCSPM design for the final upgrade of LS3.

With the proposed selection of slots, some of the installed TCSPMs risk to intercept significant beam loads during injection failures or asynchronous beam dumps. Nevertheless, HiRadMat experiments suggest that this is not an issue for the collimator robustness. Still, a minor scratch of the Mo coating could occur, but in this case the collimator can be moved using the 5^{th} axis, orthogonally to the collimation plane, to expose an undamaged surface to the beam. Since such a serious accident is considered to be very rare, this is an acceptable risk that will not have an impact on operation.

Where possible, we propose to maintain operational the TCSG collimators presently installed at least for the first year of operation in Run III; therefore, installation of the new TCSPM collimators will be in the adjacent TCSM slots. The feasibility of such a possibility depends also on the compatibility of the present controls infrastructure that would have to cope with 8 additional collimators.

References

[1] O. Brüning *et al.* (eds), "LHC design report", Vol. I, CERN, Geneva, Switzerland, Rep. CERN–2004–003–V–1, 2004.

[2] G. Apollinari *et. al*, "High Luminosity Large Hadron Collider (HL–LHC) Technical Design Report V.01", CERN, Geneva, Switzerland, EDMS n. 1833445 v.09.05, `https://edms.cern.ch/document/1833445`

[3] X. Buffat *et al.*, "MD3288 – Instability latency with controlled noise", presentation at the LSWG meeting, 3rd July 2018, CERN, Geneva, Switzerland.

[4] F. Carra, presentation at the 80^{th} Collimation Upgrade Specification Meeting (ColUSM), of Dec. 9^{th}, 2016. `https://indico.cern.ch/event/591788/`

[5] "Installation of a low–impedance secondary collimator (TCSPM) in IR7", EDMS doc. 1705738 (v.1.0), LHC–TC–EC–0006 (v.1.0) (2017).

[6] "Installation of the LUA9 Equipment in IR7 of the LHC", EDMS doc. 1329235 (v.1.0), LHC–TEC–EC–0001 (v.1.0) (2017)

[7] N. Mounet, "Impact of "old" TCSG collimators in parking position during Run III", presentation the HSC section meeting, 5^{th} November 2018, CERN, Geneva, Switzerland.

[8] "Installation in IR7 of Primary Crystal Collimators (TCPC) on Beam 2", EDMS doc. 1714148 (v.1.0), LHC–TC–EC–0008 (v.1.0) (2017).

[9] A. Bertarelli, F. Carra, N. Mariani and S. Bizzaro, "2014 Development and testing of novel advanced materials with very high thermal shock resistance", in *Proc. Tungsten, Refractory and Hardmetals Conference*, 18th – 22nd May 2014, Orlando, Florida, USA.

[10] N. Mariani, "Development of Novel, Advanced Molybdenum–based Composites for High Energy Physics Applications", Ph. D. Thesis, Politecnico di Milano (2014).

[11] E. Skordis, "Effect of non–inelastic interactions (EM and nuclear elastic) of primary protons in TCP", presentation at the LHC Collimation Working Group Meeting, 7th March 2015, CERN, Geneva, Switzerland.

[12] F. Carra, "Thermomechanical response of advanced materials under quasi–instantaneous heating", Ph. D. Thesis, Politecnico di Torino (2017).

[13] E. Metral, *et al.*, "Update on the HL–LHC operational scenarios for proton operation", CERN–ACC–NOTE–2018–0002 (2018)

[14] A. Bertarelli, "HRMT–36 (MultiMat) Experiment: Preliminary Results", presentation at the Collimation Upgrade Specification Working Group Meeting, 8th November 2017, CERN, Geneva, Switzerland.

[15] R. Bruce, *et al.*, "Parameters for aperture calculations at injection for HL–LHC", CERN–ACC–2016–0328 (2016).

[16] R. Bruce, *et al.*., "Reaching record–low β^* at the CERN Large Hadron Collider using a novel scheme of collimator settings and optics", Nucl. Instr. Meth. Phys. Res. A, 848:19 – 30, Jan. 2017

[17] D. Amorim, *et al.*, "HL–LHC Impedance and Related Effects", CERN–ACC–NOTE–2018–0087 (2018).

[18] S. Antipov, *et al.*, "Machine Impedance and HOM Power Update", 7th HL–LHC Collaboration Meeting, Madrid, Spain, Nov. 2017

[19] E. Carideo, S. Antipov, N. Biancacci, B. Salvant, "Effect of the actual taper geometry on collimator impedance and octupole thresholds of LHC and HLâĂŞLHC", presentation at the HL-LHC WP2 Meeting, 27th November 2018, CERN, Geneva, Switzerland.

[20] C. Bracco, "Commissioning scenarios and tests for the LHC collimation system", Ph.D. thesis, Ecole Polytecnique Fédérale de Lausanne (2009).

[21] A. Mereghetti *et al.*, "SixTrack–FLUKA active coupling for the upgrade of the SPS scrapers", in *Proc. 4th Int. Particle Accelerator Conf. (IPAC'13)*, Shanghai, China, May 2013, paper WEPEA064, pp. 2657–2659.

[22] "LHC Optics Web Home", `http://abpdata.web.cern.ch/abpdata/lhc_optics_web/www`

[23] R. Bruce *et al.*, “New IR7 optics with removed MQW magnets”, presentation at the Hadron Synchrotron Single Particle Dynamics section meeting, 6th December 2017, CERN, Geneva, Switzerland.

[24] R. Bruce *et al.*, “Simulations and measurements of beam loss patterns at the CERN Large Hadron Collider", Phys. Rev. ST Accel. Beams 17, 081004 (2014)

[25] A. Mereghetti *et al.*, “Tracking simulations of protons quench test”, presentation at the LHC Collimation Working Group meeting, 7th March 2016, CERN, Geneva, Switzerland.

[26] E. Skordis *et al.*, “Status of energy deposition studies for the 2015 proton and ion collimation Quench Tests”, presentation at the LHC Collimation Working Group, 31st October 2016, CERN, Geneva, Switzerland.

[27] B. Salvachua Ferrando *et al.*, “Collimation quench test with 6.5 TeV proton beams”, CERN–ACC–NOTE–2016–0015 (2016).